ACS APPLIED MATERIALS & INTERFACES

Research Article

www.acsami.org

Elementary Surface Chemistry during CuO/Al Nanolaminate-Thermite Synthesis: Copper and Oxygen Deposition on Aluminum (111) Surfaces

Cloé Lanthony,[†,‡] Mathilde Guiltat,[†,‡] Jean Marie Ducéré,[†,§] Agnes Verdier,[†,§] Anne Hémeryck,[†,§] Mehdi Djafari-Rouhani,[†,‡] Carole Rossi,[†,§] Yves J. Chabal,[∥] and Alain Estève*[,†,§]

[†]Laboratory of Analysis and Architecture of Systems, Centre National de la Recherche Scientifique, 7 Avenue du Colonel Roche, F-31400 Toulouse, France

[‡]Laboratory of Analysis and Architecture of Systems, Université Toulouse III—Paul Sabatier, F-31400 Toulouse, France

[§]Laboratory of Analysis and Architecture of Systems, Université de Toulouse, F-31400 Toulouse, France

[∥]Department of Materials Science and Engineering, University of Texas at Dallas, Richardson, Texas 75080, United States

ABSTRACT: The surface chemistry associated with the synthesis of energetic nanolaminates controls the formation of the critical interfacial layers that dominate the performances of nanothermites. For instance, the interaction of Al with CuO films or CuO with Al films needs to be understood to optimize Al/CuO nanolaminates. To that end, the chemical mechanisms occurring during early stages of molecular CuO adsorption onto crystalline Al(111) surfaces are investigated using density functional theory (DFT) calculations, leading to the systematic determination of their reaction enthalpies and associated activation energies. We show that CuO undergoes dissociative chemisorption on Al(111) surfaces, whereby the Cu and O atoms tend to separate from each other. Both Cu and O atoms form islands with different properties. Copper islanding fosters Cu insertion (via surface site exchange mechanism) into the subsurface, while oxygen islands remain stable at the surface. Above a critical local oxygen coverage, aluminum atoms are extracted from the Al surface, leading to oxygen−aluminum intermixing and the formation of aluminum oxide (γ-alumina). For Cu and O co-deposition, copper promotes oxygen−aluminum interaction by oxygen segregation and separates the resulting oxide from the Al substrate by insertion into Al and stabilization below the oxide front, preventing full mixing of Al, Cu, and O species.

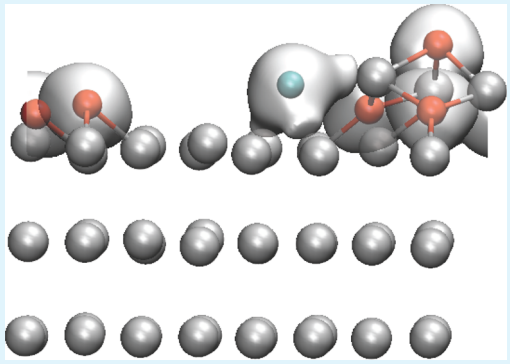

KEYWORDS: *Al/CuO nanolaminates, Al/CuO nanothermites, aluminum oxidation, DFT calculations, Cu on Al(111), Cu and O co-deposition on Al(111)*

INTRODUCTION

Nanoenergetic materials are of great interest for Micro-ElectroMechanical Systems (MEMS) technologies because they can be easily integrated, for instance in microactuators and detonators.[1,2] Their high energy density and compatibility with conventional MEMS fabrication techniques makes them ideal components of autonomous micro- and nanosystems for developing nanoenergetics-on-a-chip systems.[3] Nanolaminates (i.e., a nanofoil arrangement of thermites) composed of metal and metal-oxide (fuel and oxidizer, respectively) films allow the reactants to be intimately stacked in a controlled manner.[4] This arrangement enhances the reactivity, minimizes energy loss, and facilitates the tuning of the thermal characteristics. Among alumino-thermites or bimetallic-based nanofoils, the Al/CuO system has a relatively high energy density, 21 kJ/cm^3, that is, 3 times higher than trinitrotoluene (TNT, 7.6 kJ/cm^3), a standard high-explosive material. Importantly, it offers full compatibility with conventional microelectronics deposition processes. Therefore, CuO/Al nanofoils have attracted much attention during the past decade, as demonstrated by a number of experimental and theoretical investigations.[2,4−10]

Downscaling these materials to the nanoscale has raised many fundamental questions, such as the impact of interfaces on the thermal properties, highlighting the lack of understanding of the interface formation and motivating possible ways to design and nanoengineer smart-interfaces for tunable nanoenergetic materials.[11] In contrast to most materials, reactive stacks such as Al/CuO are intrinsically characterized by strong exothermic elementary reactions during synthesis, inevitably leading to the formation of mixed layers at the interfaces. Mixed interlayers act as barriers by slowing down mass diffusion and subsequent reactions and can stabilize the energetic material if they are uniform. The overall stability is critical and needs to be accurately controlled: a poor interfacial layer causes unexpected ignition of the thermite at relatively

Received: May 22, 2014
Accepted: August 4, 2014
Published: August 4, 2014

low temperatures, while a uniformly thick layer leads to inhibition (flegmatization) of the reaction. Controlling the atomic arrangement and thickness of the mixed region is therefore critical. For instance, the role of defects on the stability of an Al/Ni bilayer has been pointed out.[12−14] Similarly, the chemical nature of an Al/CuO interfacial layer has been shown to be more important than its physical thickness.[11] Clearly, technological and fundamental progress in such reactive heterogeneous stacked nanostructures requires understanding of the chemistry and associated fundamental mechanisms that control the formation and chemical composition of its interface, thus their impact on the performance and aging of the energetic nanolaminates.

Purely experimental studies of the interface formation are limited by the ability to analyze the chemical composition and structure with high enough spatial resolution.[7,15] Often, computational studies can not only propose and evaluate mechanisms based on hypotheses derived from experiments, but also can consider and investigate processes that are beyond the reach of experiments. For nanoenergetic materials, the theoretical efforts have primarily involved macroscale models (mainly for the Ni/Al system) and have been focused on deriving the macroscopic thermal properties and understanding the impact of intermixing on reaction velocities[16,17] and alloy formation reactions.[18] In contrast to Ni/Al, there have only been a few studies of the Al/CuO systems, combining experiments to elucidate reaction paths[8] and theoretical work to build macroscale models for its combustion.[19,20]

At the atomic scale, molecular dynamics (MD) has been used to study nanolaminates, focusing on the intermixing process at the interfaces of the nanolayers during ignition.[21,22] For instance, the role of defects in initiating the intermixing process at the Al/Ni interface[12,13,23−25] and the specific chemical mechanisms to explain atomistic exchanges at the Fe_2O_3/Al interface[26,27] have been investigated. These atomic scale studies are all based on model systems in which the interfaces are generated through crystallographic coincidence lattice site models. No attempt has been made so far to develop simulations that deal with realistic interfaces before tackling thermal studies. General methodologies have been proposed to model vapor deposition processes, addressing the basic chemical mechanisms through first-principles tools.[28] But literature dealing with specific issues associated with nanoenergetic materials (i.e., energetic reactions) is scarce, in particular for the Al/CuO nanothermite system.

This work addresses the early stages of the deposition chemistry of CuO onto Al(111) surfaces (ideal model system for real PVD experiments) using first-principles density functional theory (DFT) based calculations. We show that CuO dissociates upon adsorption, leading to Cu and O cluster formation through Cu−O repulsive forces, which induces Cu incorporation into Al and Al extraction by oxygen at high enough local coverages. Oxygen agglomeration is consistent with thermodynamic considerations,[29] even at low coverages. However, we show that calculation of kinetic barriers is critical to modeling the underlying elementary processes, such as migration and aggregation, and to examine in detail the simultaneous deposition of oxygen and copper atoms on the Al(111) surface.

This paper is organized as follows. The first section describes the computational method. The next section discusses results and addresses the adsorption and decomposition of CuO molecules on Al(111) surfaces and the individual interactions of oxygen and copper, before considering their co-deposition. The motivation for separating oxygen and copper deposition arises from experimental observation that CuO adsorption is dissociative.[5,7] In the Results, section 1 focuses on the decomposition of CuO, and section 2 focuses on the deposition of copper atoms onto Al(111) surfaces. The potential diffusion of Cu atoms into Al and their clustering either on the surface or in the subsurface[30] are also examined. Section 3 addresses the deposition of oxygen onto Al(111) surfaces, providing a kinetic confirmation of island formation at the surface, critical for subsequent oxidation.[3] Section 4 considers the simultaneous deposition of Cu and O. The results are compared with those obtained in sections 2 and 3 to assess the synergistic effect of these species on the global reactivity. Finally, conclusions and some perspectives are reported, highlighting the impact of this work for all aluminum-based technologies.

COMPUTATIONAL METHODS

All calculations presented here are based on the DFT approximation. We used the Perdew−Burke−Ernzerhof functional[31] in the Generalized Gradient Approximation (PBE-GGA) implemented in the VASP 5.2 package (Vienna Ab initio Simulation Package).[32−35] A plane-wave basis set for the Kohn−Sham Bloch functions is used, with an energy cutoff of 400 eV, to account for the valence electrons and a Monkhorst−Pack[36] mesh of 2 × 2 × 1 *k*-points for the sampling of the Brillouin zone. Projected-augmented waves are used for the representation of inner shell electrons. All performed calculations are spin-polarized, and initial magnetic moments have been introduced for systems that include copper atoms. An Al(111) slab is constructed based on an orthorhombic supercell containing six layers of 16 aluminum atoms each. Within each Al slab, the bottom layer is held fixed in the bulk configuration so as to reproduce the bulk behavior. A 15 Å thick vacuum space is added in the *z* direction for creating (111) surfaces. The total dimensions of the asymmetric orthorhombic simulation box are 11.43 × 9.90 × 25.00 $Å^3$.

An Al(111) surface exhibits two types of stable adsorption sites, namely the fcc and hcp sites, as shown in Figure 1.[29,37,38] They are

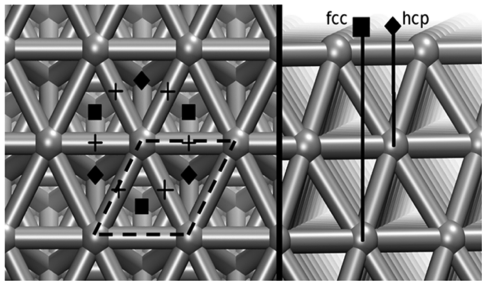

Figure 1. Different types of adsorption sites on the Al(111) surface: (■) fcc, (◆) hcp, and (+) bridge. Dashed lines represent the surface unit cell as defined in this article; (left) top view and (right) side view. Gray spheres are aluminum atoms.

associated with two possible types of stacking on a (111) surface of an fcc lattice: (i) the normal fcc stacking as obtained in epitaxial layer growth, and (ii) the hcp resulting in a stacking fault in the fcc lattice. As shown in Figure 1, the Al atom below an hcp site in the vertical direction is situated in the first subsurface layer, while for an fcc site, the Al atom is situated in the second subsurface layer. In addition to these two sites, a metastable site can be observed at the transition state between fcc and hcp, on top of the Al−Al bond center, interacting directly with these two Al surface atoms. This site is labeled as the bridge site in Figure 1. The lower coordination number explains the lower stability of this particular site. Note that each unit cell in Figure 1 comprises an fcc and an hcp site (whose distance is only 1.6 Å, which

is roughly in the order of a diatomic molecule and therefore too short to accommodate a CuO molecule, for instance).

Looking into thermodynamic characteristics, we can associate an enthalpy change with each reaction. The energy reference is taken as the Al(111) substrate alone with all other species at infinite distance. The enthalpy change is calculated as the binding energy associated with the configuration resulting from the reaction, expressed as $E = E_{total} - (E_{adsorbate} + E_{surface})$, where E_{total} is the total energy of the system in its final configuration after total energy minimization; $E_{adsorbate}$ and $E_{surface}$ are the respective energies of the isolated adsorbate and the surface slab alone. Kinetic rates are derived from the activation energy barriers, which are the enthalpies at the saddle points for the transition between two configurations. A saddle point is obtained through the determination of the minimum energy pathway, among all possible pathways in the multidimensional space. In this study, the nudged elastic band (NEB)[39−41] method is used to find these pathways and the related energy barriers.

RESULTS

1. Copper Monoxide Adsorption and Decomposition on Al(111). The interaction of copper monoxide with the Al(111) surface is examined first. Copper monoxide is the most stable gas product expected from the sputtering experiment. Considering the three high symmetry sites of the surface (fcc, hcp, and bridge), three initial positions of the CuO molecules are tested with the CuO molecule positioned at distance of 3 Å (i.e., far enough from the Al surface layer) with its molecular bond axis parallel to the surface to enable reorientation of the molecule during energy minimization. For instance, two of these initial positions have the CuO molecule positioned above the surface with its oxygen atom on top of the fcc site and the copper atom on top of the hcp site, and vice versa. This makes it possible to examine the competition between the respective affinity of copper and oxygen to the aluminum surface to determine the lowest energy adsorption state. In the third position, both copper and oxygen atoms are on top of the adjacent bridge sites.

In the first two cases, a direct and fully dissociative chemisorption is observed, as illustrated in Figure 2 (panels a and b are the initial and final states, respectively). In both cases, the oxygen atom is adsorbed remaining in its initial axis, either fcc or hcp, and the copper atom migrates toward a bridge site away from the oxygen adsorption site (d_{Cu-O} = 3.7 Å), that is, with the Cu atom crossing over into the next neighboring unit cell (repulsed away). These two adsorption configurations have different adsorption energies: when the O atom remains on top of fcc site, which appears to be the most favorable configuration, the adsorption energy is large (−6.97 eV); in contrast, when the O atom is adsorbed on an hcp site, the chemisorption energy is reduced to −6.57 eV, that is, +0.4 eV above the most stable configuration. These results are in agreement with previous findings of the most stable adsorption sites for isolated oxygen atoms,[42−45] leading to the conclusion that the oxygen atom is driving the thermodynamics of CuO decomposition. To quantify this repulsion and resulting chemical separation of copper and oxygen atoms, a static calculation is performed to compare the energies of O and Cu atoms in similar sites (both in fcc or both in hcp) but adjacent unit cell (separation of 2.7 Å; d_{Cu-O} = 2.7 Å) with the corresponding energies when the Cu atoms migrate to adjacent bridge sites (separation of 3.7 Å). The former configuration, which could intuitively correspond to the most favorable dissociative chemisorbed state, (with d_{Cu-O} = 2.7 Å) is characterized by a −6.29 eV adsorption energy, less stable

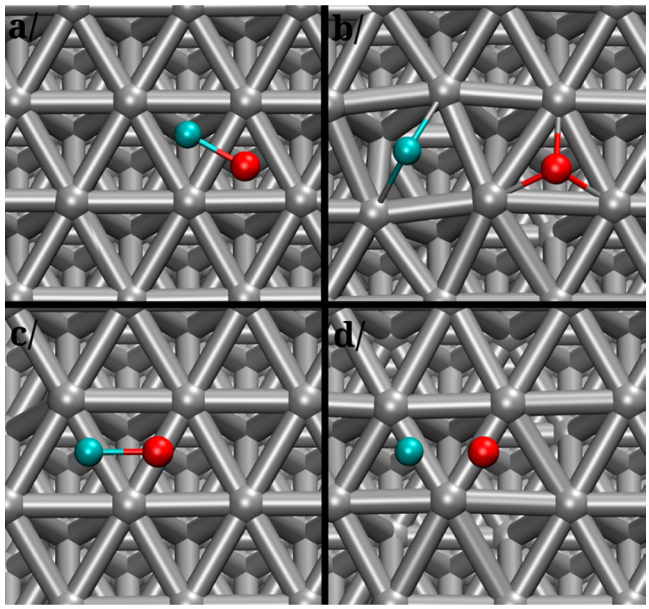

Figure 2. Top views of two different adsorption states of CuO on Al(111). (a) Initial and (b) final configurations of the dissociative adsorption; (c) initial and (d) final configurations of the partial-dissociative chemisorption. Gray, blue, and red spheres are aluminum, copper, and oxygen atoms, respectively.

than the two previous geometries obtained after dissociation (with d_{Cu-O} = 3.7 Å).

In the third position, wherein both copper and oxygen atoms are on top of the adjacent bridge sites, the molecule−surface interaction is weaker, with a −2.92 eV adsorption energy. Here, only partial CuO molecular dissociation is observed (Figure 2c,d). This chemisorbed state is characterized by an increase of the Cu−O molecular bond length to 1.79 Å from its gas phase value of 1.66 Å. Furthermore, the equilibrium position of the CuO molecule is far from the surface (2.4 Å), compared to the distance of the dissociated states, with typical $d_{O-surface}$ values of ∼0.80 Å for both fcc and hcp sites and $d_{Cu-surface}$ values of ∼1.60 Å for the same sites. Note that the distance between the Cu atom and the surface plane is reduced to 1.50 Å for the bridge case. This metastable bridge state can be seen as a possible step in the pathway from the gaseous phase toward a full dissociation of CuO, as previously discussed. The transition from this metastable chemisorbed state to the full dissociative state can probably take place without any incubation time at normal processing conditions, because a slightly nonsymmetrical initial positioning of the CuO molecule leads to full dissociation. These data lead us to the conclusion that CuO in its molecular form has no appreciable lifetime in contact with the Al(111) surface.

Additionally, initial vertical positions for the CuO molecules on top of the surface have also been tested (on either side of the molecule facing fcc or hcp sites). In all cases, full decomposition is observed with no fundamental change from what is observed in the cases of parallel positionings.

To better understand CuO adsorption, we calculated the adsorption energies of isolated O and Cu atoms on two different Al(111) slabs, starting with isolated O in an fcc position and isolated Cu in a bridge site. The total energy gain with respect to molecular CuO as reference amounts to −6.94 eV. This value is comparable to −6.97 eV already found in the first case examined in this section, when a CuO molecule was

deposited on the same substrate, resulting in the Cu and O atoms separated by 3.7 Å.

This finding indicates that the interaction with the Al(111) surface can be studied separately, in the limit of low coverage (initial exposure), because there is no significant chemical interaction between the two adsorbed species (Cu and O) when positioned in adjacent neighboring sites (i.e., no energy stabilization). Therefore, the next section focuses on separate studies of adsorption and migration of isolated Cu and O atoms before examining the more complex case of co-deposition. This choice is also consistent with experimental procedures, because the CuO target surface is likely to decompose into Cu and O before evaporation when hit by highly energetic Ar^+ ions in the usual plasma sputter-deposition technique.[5,8]

2. Copper on Al(111). *Surface Clustering.* In this section, we consider copper deposition on the Al(111) surface. The calculations described above indicate that the adsorption on fcc, hcp, and bridge Al(111) surface sites is energetically equivalent, with respective binding energies of 2.78, 2.77, and 2.72 eV. In fcc and hcp configurations, three Al−Cu bonds are formed with equivalent 2.42 Å bond lengths, whereas the Cu bridging configuration exhibits four Cu−Al bonds, two short bonds (2.35 Å) that contribute mostly to the stability and two long bonds (2.67 Å) associated with weaker interactions with second Al neighbor atoms. Interestingly, an investigation of the migration pathways between these three sites reveals that the activation barriers are low, indicating that copper atoms move quasi freely on the Al(111) surface even at low temperatures. The activation barriers are displayed in Figure 3 for migration

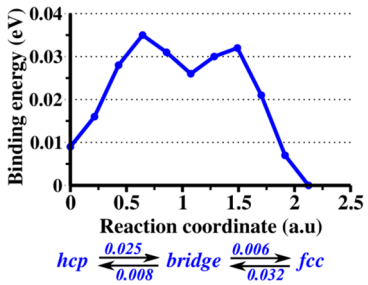

Figure 3. Activation barriers encountered along surface migration of copper atom on an Al(111) surface, between fcc, hcp, and bridge sites as described in Figure 1. Reference energy given in eV is taken for Cu in fcc site as the most stable configuration. Activation barriers (in blue) are given in eV.

from the fcc to the hcp sites through the bridge configuration. They are all in the range of 0.01−0.03 eV, which is the same order of magnitude as k_BT = 0.025 eV at room temperature. This behavior can be explained by the metallic nature of the Cu/Al(111) interaction, which consists in the integration of the copper electronic wave functions into the delocalized electron gas of the aluminum surface, leading to similar energies for the different sites (fcc, bridge, and hcp) with negligible barriers in between. We conclude that the binding energy of copper atoms is not sensitive to the local configuration of the neighboring Al atoms.

We now consider the properties of a second Cu atom adsorbed in an fcc, hcp, or bridge site in the vicinity of an existing Cu atom. We find that the bridge configuration is not stable, leaving only the adjacent hcp or fcc site as possible neighboring configuration depending on the position of the original Cu atom. Table 1 reveals that when the Cu coverage is

Table 1. Adsorption Energy of Copper Atom Positioned in fcc and hcp Close Packed Configurations[a]

	number of packed Cu				
	1	2	3	4	5
E_{ads} on fcc (eV per atom)	−2.78	−2.95	−3.08	−3.18	−3.25
E_{ads} on hcp (eV per atom)	−2.77	−2.94	−3.05	−3.17	−3.23

[a]Adsorption energy gains are given per deposited Cu atom (in eV).

increased, clustering with either a local hcp or fcc configuration is favored, indicating that there is a strong coupling energy between the surface Cu atoms. Indeed, when Cu atoms are on neighboring sites, the adsorption energy per atom inside the cluster increases with cluster size, up to a non-negligible value (e.g., 0.47 and 0.46 eV per atom gained for clusters of five Cu-fcc and Cu-hcp configurations, respectively). A NEB calculation was also performed to estimate the activation barriers for Cu atom extraction from a four Cu cluster. In this process, a Cu atom is moved away from the rest of the cluster by one first neighbor position, either fcc or hcp, which places it at least at a second neighbor position from other Cu atoms inside the cluster. Similar to the case of the Cu-bridge position at the proximity of other surface copper atoms, these second neighbor sites are unstable, and the Cu atoms extracted from the copper clusters recover their initial positions inside the cluster after relaxation. As a result, we estimate that the activation barriers for extraction is ∼0.5 eV for hcp and fcc sites, as the barrier for further migration of the isolated copper atoms is negligible compared to its aggregation energy (energies given for the extraction from a five Cu cluster and referenced to an isolated copper atom on the surface).

Copper Site Exchange Process. In addition to surface migration, an adsorbed Cu in either fcc or hcp position can exothermically insert into the aluminum slab, by Al substitution (i.e., extraction out of its original surface lattice site to above the surface). The successive steps of this "site exchange" path are shown in Figure 4. The initial state (Figure 4, left) corresponds

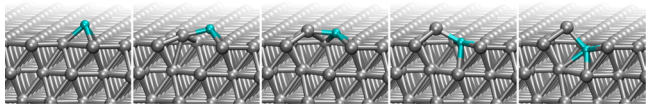

Figure 4. Side views of pathway of (blue spheres) copper insertion into Al(111), associated with a barrier of 0.54 eV.

to the adsorbed Cu atom, the transition state (4, center) shows the Cu and Al atoms both out of the surface, and the final state (Figure 4, right) illustrates the final position of the copper atom within the Al surface layer. This favorable site exchange process occurs through a concerted movement between the copper and extracted aluminum atom and is characterized by an activation barrier of 0.54 eV in the case of a single copper atom interaction. The reaction is slightly exothermic with an enthalpy of −0.12 eV (Table 2). The activation barrier decreases when the environment is copper-rich, as illustrated by the data given in Table 2. Two situations are examined: (i) adsorption next to an existing surface Cu atom, and (ii) adsorption next to a subsurface Cu atom. The corresponding activation barriers are lower (0.45 and 0.40 eV for i and ii, respectively) and the enthalpies larger (−0.22 and −0.14 eV, respectively). This thermally activated concerted mechanism is confirmed by a molecular dynamics simulation performed at T = 300 K,

Table 2. Energy Gains, Insertion Energies, and Activation Energies Given for Various Copper Adsorbed Configurations and Insertion Paths for Cu-fcc Atoms[a]

initial configuration	final configuration	energy gain (eV)	insertion energy (eV)	activation energy (eV)
1 adsorbed Cu-fcc	inserted Cu	−0.12	−2.90	0.54
2 adsorbed Cu-fcc	1 inserted Cu + 1 adsorbed Cu	−0.22	−3.36	0.45
1 adsorbed Cu-fcc + 1 Cu inserted	2 inserted Cu	−0.14	−3.48	0.40

[a]For the single copper atom configurations, the reference in energy is the substrate plus copper atom at an infinite distance from it. For the two copper atom configurations, the reference becomes an adsorbed copper atom configuration plus another copper atom considered at an infinite distance. Only Cu-fcc adsorbed sites are given in the table.

showing a shorter time for penetration (t = 3 ps) compared to that of a single Cu atom, without adding any extra force or interaction on the system during the simulation.

These results indicate that under low pressure conditions, isolated copper atoms will either penetrate into the substrate or migrate freely on the surface until they meet each other. Because surface migration leads to island formation due to the attractive nature of Cu−Cu interaction on Al(111) surfaces, the local coverage of Cu will increase and favor substitution of surface Al atoms with copper atoms, thanks to the favorable cooperative effect (decrease of the activation barriers). These findings are consistent with the conclusions reported in the literature and derived from experiments on the deposition of Cu on Al(111) analyzed by Auger electron spectroscopy and transmission electron microscopy (TEM).[46−48] The various observations made on thin Cu films deposited on Al indicate that (i) the adsorption of the first atomic layer shows long-range disorder, with the appearance of Cu(111) islands, and (ii) during the deposition of the second atomic layer, the first one penetrates the aluminum substrate and disappears completely. Thus, intermixing occurs very rapidly, so that an alloy is formed during the deposition process.

3. Oxygen on Al(111). This section describes the two successive regimes associated with the deposition of oxygen on Al(111):[43,49] (i) the adsorption regime limited to the surface (adsorption without penetration), and (ii) the oxidation regime in which aluminum extraction takes place. For the first regime, there is no oxide created and no real mixing of Al and O species. In contrast, the second regime involves intermixing of both oxygen and aluminum, as previously noted.[37]

Adsorption Regime, Surface Clustering. For the adsorption of a single oxygen atom on the aluminum surface, the fcc site (E_{ads} = −7.64 eV) is more stable than the hcp site (E_{ads} = −7.24 eV). In contrast to an isolated Cu atom, an oxygen atom is not stable on the bridge site that now corresponds to the saddle point for migration from the fcc to hcp sites and vice versa. The associated activation barriers are 0.72 eV for fcc-to-hcp migration and 0.32 eV for the back migration.

The adsorption of molecular oxygen has been theoretically[38,50−54] and experimentally[43] reported. There is a consensus that it spontaneously and exothermically dissociates resulting in hyperthermal displacement. While static DFT calculations indicate that neighboring fcc sites are favorable after dissociation,[38] surface separation resulting from hyperthermal trajectories during dissociation may lead to isolated configurations for the surface oxygen atoms. Consequently, consideration of isolated oxygen atoms is most appropriate in the limit of early oxidation stages and low pressure conditions, the utilization of molecular O_2 in our investigation should rise to the same general conclusions. At higher coverage or longer times, islanding needs to be considered as static DFT calculations and experiments on higher surface coverages indicate that oxygen atoms interact on the surface and have the propensity to form ordered islands, thanks to activated migration of oxygen atoms. For instance a (1 × 1) pattern is observed and corresponds to an epitaxial arrangement of a single oxygen monolayer on the (111) aluminum surface. These findings were first revealed by Brune's scanning tunneling microscopy (STM) real-time observations of aluminum surface oxidation,[43,44,49] and have since been confirmed by other experimental[55] and theoretical[52,53,56] studies.

We now examine in more detail this tendency for oxygen to agglomerate on the surface. An incremental method is applied to model the assembly of one to seven oxygen atoms into islands, which corresponds to almost a half-monolayer coverage for the 16 Al atoms used in a surface unit-cell. In these calculations, we consider different sizes of closed-packed oxygen-fcc islands and calculate the activation barrier required for one oxygen atom to leave the islands (i.e., from its close packed fcc site to an adjacent hcp site). Figure 5 (top) shows

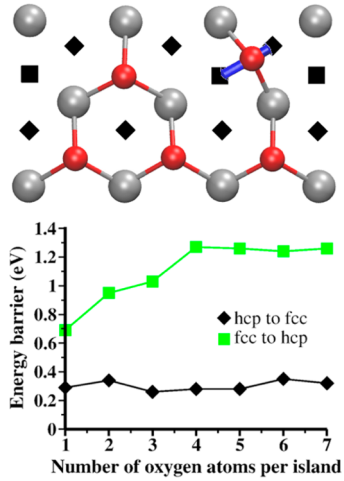

Figure 5. Group effects for adsorbed oxygen atoms on Al(111). (Top) Top view of migration pathway investigation through NEB calculations, with fcc sites represented by squares, and hcp by diamonds in the case of a five oxygen atoms island. (Bottom) Graph of both-ways migration barriers occurring at the edge of the island as a function of the island size.

the calculation performed on a five oxygen-fcc island, and Figure 5 (bottom) summarizes the results that include activation barriers for both leaving the cluster and reagglomerating into the cluster.

We previously showed that for a single oxygen atom migrating on the surface, the energy barrier for migrating from an hcp site to an fcc site is 0.32 eV, and the energy barrier for the way back is 0.72 eV ; hence, oxygen atoms tend to remain on fcc sites once adsorbed or after migration from adjacent hcp sites. This calculation justifies the close-packed arrangement of oxygen-fcc atoms on Al(111) surfaces.

When increasing the island size from two to seven oxygen atoms, the fcc to hcp activation barrier rapidly increases to 0.9,

1.0, and 1.3 eV for two, three and four oxygen atoms island size, respectively. For island sizes beyond five oxygen atoms, this barrier reaches a 1.3 eV energy plateau, as can be seen on the graph in Figure 5 (black ◆). Interestingly, for all coverages, the hcp to fcc back reaction barrier (green ■, Figure 5) fluctuates slightly around an average value of 0.3 eV, similar to the barrier for isolated hcp to fcc migration. Hence, hcp to fcc oxygen migration is a favorable mechanism, easily taking place at room temperature and independent of oxygen coverage. Similar to the case of copper, the total adsorption energy of two agglomerated oxygen atoms in first neighbor positions increases by 0.2 eV when compared to second neighbor oxygen atoms. In contrast to Cu, however, there is no interaction between the oxygen atoms, that is, the adsorption energy remains independent of O−O distance.

Adsorption versus Insertion. The high binding energy of oxygen to aluminum has led to the assumption that oxygen can easily penetrate into aluminum to form an oxide. Indeed, several studies[57−59] on the subject have suggested and even concluded that oxygen insertion in aluminum is central to aluminum oxidation. However, our recent calculations have shown that oxygen insertion in the aluminum subsurface is not likely to happen at the initial stage of oxygen exposure because of both thermodynamic and kinetic considerations.[37] In the following, we demonstrate that the oxidation of aluminum is not mediated by an initial insertion of oxygen atom into the aluminum subsurface but rather by Al extraction through cooperative oxygen effects at the surface.

First, we compare the energy for adsorbing an oxygen atom on the Al(111) surface to that for inserting it into the first aluminum subsurface layer, focusing on the neighborhood of close-packed oxygen islands of sizes varying from 0 oxygen (no island) up to 15 oxygen atoms. This range for the total oxygen coverage (i.e., the total number of oxygen atoms from 1 to 16 atoms), represents 0 to 1 full monolayer (1 ML). Figure 6

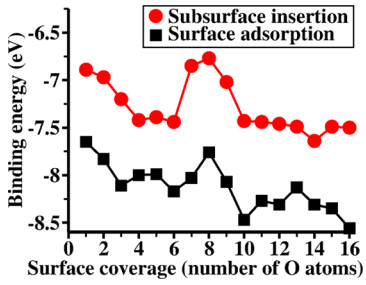

Figure 6. Adsorption to grow (1 × 1) island (black ■) versus insertion (red ●) formation energies as a function of surface island size. In the red curve, at each red ●, a single oxygen atom is inserted.

reports the incremental adsorption and insertion energies as a function of the total oxygen coverage. It is clear that the adsorption to form an oxygen (1 × 1) surface pattern is always energetically more favorable than top insertion of an oxygen atom by 0.7 to 1.0 eV. To examine the kinetic aspects of the process, we perform an NEB calculation to find the insertion pathways in the absence or presence of oxygen islands on the Al(111) surface. Figure 7 illustrates the resulting reaction path for the insertion of an isolated oxygen atom, starting from an fcc site and ending in a subsurface tetrahedral site. This reaction is endothermic, as shown in Figure 7, with ΔE = +0.72 eV. The activation energy is too high ($E^{\ddagger}$ = 1.73 eV) to occur at room temperature. Furthermore, the calculations show that the

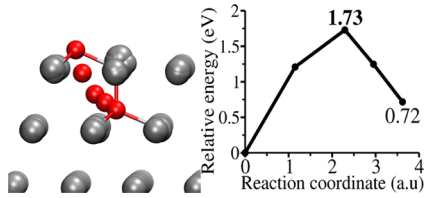

Figure 7. Insertion path for one oxygen atom from an fcc adsorbed surface site to a tetrahedral subsurface inserted configuration, as obtained during the NEB calculations. Energy reference is taken in the starting surface adsorbed fcc configuration. Final state corresponds to oxygen atom inserted in the subsurface.

activation energies for insertion of an oxygen atom from a 5 O-(1 × 1) island up to a full monolayer O-(1 × 1) are even higher than 2 eV. Therefore, direct insertion of oxygen into the aluminum subsurface does not play a significant role in initiating aluminum oxidation at room temperature.

In the following section, we discuss the Al/O mixing mechanism for oxide nucleation, which, contrary to general assumptions, occurs through the extraction of aluminum atoms from the surface layer into the oxygen island thanks to a cooperative effect of the oxygen-(1 × 1) pattern.

Oxidation Regime, Nucleation Mechanism. It has been found that the aluminum oxidation process starts with a nucleation phase at random points of the surface, continues with the growth of these oxide nuclei, and finally spreads all over the surface to recover it with a thin oxide layer.[51,57,58] The dependence between the beginning of the nucleation process and the oxygen coverage has not yet been determined, and contradictory hypotheses have been proposed.[51,57,58] From this prior work, there is evidence that the oxidation can start as soon as the oxygen atoms agglomerate on the surface into islands. Brune's results suggest that three environments coexist on the surface during the early stages of deposition: bare Al, oxygen-(1 × 1) islands, and oxide nuclei.[49]

To examine the mechanistic steps of oxygen adsorption after low exposure to oxygen atoms or molecules, we add more oxygen atoms on the substrate by either adsorbing them on a free Al site (clean area) or on top of an oxygen island. In the latter case, Figure 8 illustrates the main finding that the addition

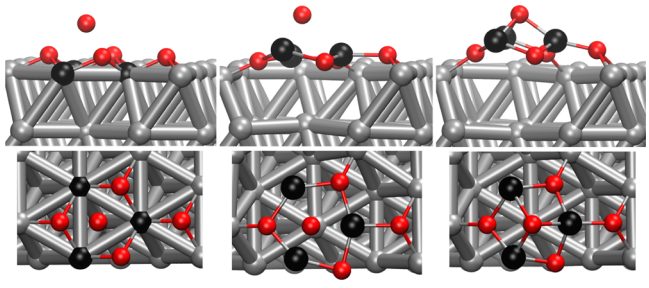

Figure 8. Extraction mechanism in three steps, (top) side views and (bottom) top views. Extracted Al atoms are black.

of an adatom of oxygen directly leads to the extraction of aluminum atoms through a barrierless chemical process.[37] In this calculation, an oxygen atom is initially deposited above an island containing four oxygen atoms. The deposited oxygen atom then interacts with three surface aluminum atoms, which are pulled out from their original lattice positions, that is, they "percolate" through the surface oxygen atoms (island) and finally stabilize above it. This process, labeled as "extraction

mechanism", leads to the formation of tetrahedrally bonded aluminum to oxygen, similar to alumina, on top of a nonoxidized aluminum surface. The top view clearly shows the upward movement of the three Al atoms, without disturbing the neighboring atomic arrangement. Figure 8 also shows the Al atoms bond with the oxygen adatom (with an Al−O bond length of 1.88 Å) with complete loss of all Al−Al bonds, underscoring the chemical changes (oxidation). These three Al atoms lose their metallic coordination in the slab and become isolated and oxidized. They constitute the first oxide nucleus.

The calculations show that this extraction mechanism is barrierless and highly exothermic (e.g., with an energy gain of −5.6 eV for a four-oxygen atom island). The process starts as soon as one oxygen atom is deposited on top of an oxygen island containing at least three oxygen atoms. The oxide nucleus thus formed is stable, despite the formation of three holes in the original aluminum layer created by the upward motion of three Al atoms. At this stage of the process, there is no global amorphization or complex atomic rearrangement, although the charge isosurfaces do indicate the presence of a vacancy in the metallic electronic density (Figure 9). This process therefore leads to a very symmetrical structure that constitutes the initial nucleus of oxidation, as indicated by the Al−O bond lengths and local structural arrangement (Figure 8). No reconstruction is seen around the extracted positions, leaving well-defined void structures.

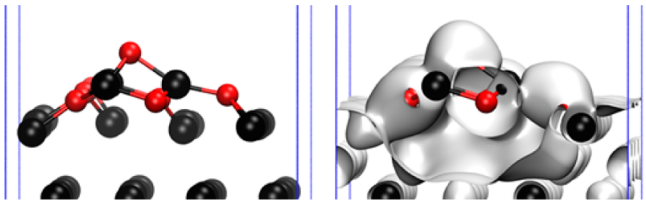

Figure 9. (Left) Upper part of the slab with an oxide nucleus; (right) electronic charge density associated with the oxide nucleus (0.15 electron/Å3). (Black) Al atoms, (red) oxygen, and (blue lines) lateral limits of the simulation box.

Beyond the Monolayer Coverage. The above extraction mechanism constituting the origin of aluminum oxidation is investigated more thoroughly by adding oxygen atoms on the previous surface, up to 2 ML coverage, and the results summarized in Figure 10 (note that 1 ML = a total number of 16 oxygen atoms). Our method is incremental, equivalent to the one presented previously in Figure 6. An extra oxygen atom is added to a pre-existing oxygen island on the surface either on the side or on top of it; the oxygen adsorption on either clean or oxygen-covered aluminum surface (Figure 10, black ■) is examined and the aluminum extraction from surface to the oxygen layer (Figure 10, orange ◆) mechanisms considered. Therefore, all calculations are independent from each other; the initial island shape is chosen to offer a maximized compactness. After minimizing the total energy of the system, we calculate the formation energy to bring an oxygen atom from infinity to the substrate and compare the two mechanisms (oxygen addition on the side and on top of a cluster). Importantly, adding an oxygen atom on top of the oxygen cluster is accompanied by the extraction of three aluminum atoms from the surface, as described in the previous section. We find that this second mechanism, associated with aluminum extraction, is always thermodynamically less favorable than the simple adsorption of oxygen on the side of an oxygen cluster by roughly 1 eV. Therefore, while completing the oxygen layer is energetically favorable, statistically, there will be a fraction of the oxygen landing on the existing oxygen clusters and then immediately fostering aluminum extraction because that process is barrierless.

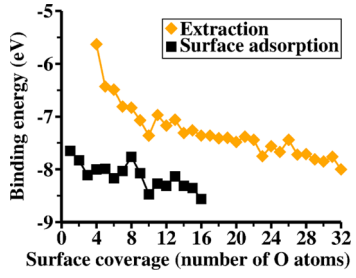

Figure 10. Extraction (orange ◆) vs adsorption (black ■) binding energies on the oxygen surface coverage. Oxygen adsorption curve is stopped at 16 O atoms because a full monolayer is reached at this stage.

For oxygen coverages over 1 ML (up to 2 ML), the incremental extraction energy decreases slightly with increasing cluster size but always remains higher than the insertion energy.[31] However, kinetics favors the extraction mechanism. The high energy barriers for the oxygen insertion (>2 eV) make them highly improbable at room temperature. Results are reported in Figure 10 for 16−32 oxygen atoms. Consequently, the oxide nuclei formation is governed by the probability of oxygen molecules arriving from the gas phase on top of an existing oxygen island. These findings are in agreement with more recent MD calculations[51] and consistent with earlier experimental work showing that at low temperatures (i.e., limited oxygen migration) island formation obeys percolation rules and the oxide nuclei forms at roughly 0.5 ML coverage.[43,49] At high temperatures, the oxygen migration was determined to be fast with rapid island formation. Overall, the oxide nucleation process itself was observed to occur at low coverages and to depend on experimental conditions, such as deposition temperature and oxygen partial pressure, which control the migration and the deposition processes.

We now consider the structural aspects of the surface after oxygen adsorption and aluminum extraction. The 16 atom oxide/Al surfaces used in our static calculations are not sufficient to represent macroscopic size substrates, and so, a close examination of the local structures is useful to compare with state-of-the-art structures published to date in the literature. While the structure obtained after direct exposure of 2 ML on the Al(111) surface (final structure shown in Figure 11) appears disordered, a careful examination reveals that the associated oxidation process leads to a structure close to gamma-alumina (γ-Al_2O_3). For instance, the characteristic alignment of octahedra and tetrahedra are found in the oxygen atoms surrounded by Al atoms (shown in purple and gray, respectively, in Figure 11), with a typical alternation of small and long Al−O bonds, with d_{Al-O} = 1.73 to 1.77 Å and d_{Al-O} = 1.83 to 1.89 Å, close to the known values of 1.76 and 1.83 Å, respectively.[60] This nonperfect, substochiometric structure points to the formation of a very thin layer of "γ-like-Al_2O_3" at the early stage of aluminum oxidation, consistent with previous experimental studies.[61−63] Furthermore, the resulting oxide/Al layers derived from our calculations are energetically

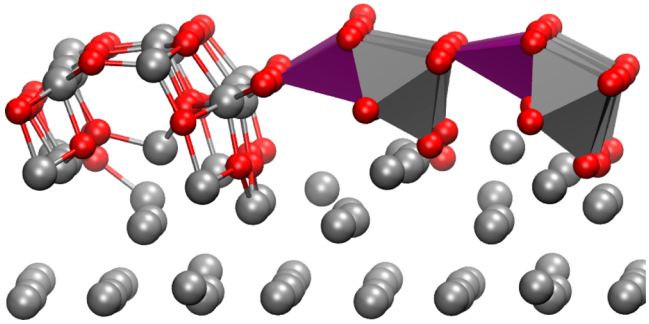

Figure 11. Resulting structure of the oxidation with 2 ML of oxygen. (Left) Raw representation; (right) highlight of the local order and symmetry with purple tetrahedra and gray octahedra.

more favorable by 0.25 eV per oxygen atom than the oxide layers proposed by Lundqvist and co-workers, wherein oxygen atoms were positioned below the top aluminum atoms (i.e., inserted into the Al layer rather than extracted).[58] At roughly half extraction of the surface aluminum layer, the well-defined voids associated with the extracted Al atoms tend to vanish due to the swelling of the oxide layer that find chemical connections to the aluminum layer underneath the extracted layer. Finally, for completeness and to explore potential artifacts due to the finite unit-cell size, we have also performed room temperature MD calculations on a repeated 2 × 2 unit cell representation of the surface and confirmed that there is no change in the atomic arrangement of the oxide layer.

In summary, oxygen atoms deposited on a bare Al(111) surface first adsorb exothermically and preferentially on fcc sites ($E^{\ddagger}$ = −7.64 eV). The activation barriers for migration from fcc and hcp sites are reasonably low (fcc-to-hcp = 0.7 eV, hcp-to-fcc = 0.3 eV) leading to aggregation into islands. Once agglomerated into islands, the adsorbed atoms cannot go back to the isolated oxygen configurations due to attractive interactions that stabilize the islands. Furthermore, the only reaction in competition with oxygen adsorption and migration on the surface is the aluminum extraction mechanism leading to the formation of an oxide nucleus, because the oxygen insertion in subsurface is endothermic and associated with a high activation barrier. This oxide nucleation is exothermic and barrierless and can begin as soon as oxygen islands exist on the surface (i.e., an additional oxygen lands on such an oxygen island). If a newly deposited oxygen atoms arrives on a clean Al surface patch, it migrates to the side of an island. If it arrives on top of an island, it extracts three Al atoms from the surface. Up to a 2 oxygen ML coverage, a thin oxide layer is formed on top of the aluminum surface, identified as a γ-like-Al_2O_3 structure, consistent with all previous experimental studies. However, this extraction mechanism is only dominant during the very first stages of aluminum oxidation. Once the thin oxide layer is formed, other mechanisms will take over, including the penetration of new oxygen atoms through the oxide layer to reach the metallic aluminum and to oxidize it deeper. This regime is beyond the scope of this work.

4. Copper and Oxygen on Al(111). We showed in the previous sections that copper and oxygen, upon CuO adsorption, tend to separate on Al(111) surfaces. Oxygen atoms agglomerate leading to aluminum extraction and formation of aluminum oxide nuclei. The copper atoms form islands, preferentially in the subsurface region. This situation holds at low coverage, where enough space is available for the formation of separate oxide nuclei and copper islands. With increasing coverage, the oxide nuclei and copper islands will eventually coalesce. Prior to coalescence, isolated migrating O or Cu species can interact with copper or oxygen-rich zones, respectively. To study these effects, we investigate the co-deposition of copper and oxygen atoms on Al(111) surfaces, using two model systems corresponding to copper- and oxygen-rich substrates that are derived from previous sections on Cu and O exposures treated separately. First, we concentrate on the configurations in which Cu atoms are in the neighborhood of an oxide nucleus. Then, we focus on how oxygen atoms behave in the vicinity of a copper-rich zone. Specifically, we investigate whether Al oxidation persists through the extraction mechanism even in the presence of copper.

Copper Reactivity with Oxide Nuclei. A model-Al surface is constructed with 16 surface aluminum atoms and 6 oxygen atoms (5 in the first layer and one additional on top) that form an oxide nucleus. This moderate oxide nucleus size is sufficient to represent an oxide yet leave enough bare aluminum to prevent interaction between different oxide nuclei present in repeated cells, when applying periodic boundary conditions. Several initial positions of the added copper atom around the oxide nucleus are considered in order to map the different possible copper -to-island interactions (see Figure 12). Four

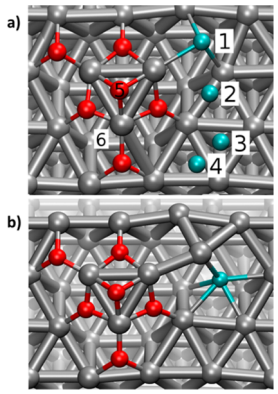

Figure 12. Adsorption and insertion of copper atom in the vicinity of oxide nucleus. (a) Initial adsorbed copper atom positions tested; (b) copper atom after insertion. Gray, blue, and red spheres are aluminum, copper, and oxygen atoms, respectively.

positions of the Cu on top of the Al surface (labeled 1−4 in Figure 12) are initially tested. Other positions are also tested on top of(labeled 5 in Figure 12) and below (labeled 6 in Figure 12) the oxide nucleus (i.e., in the vacancy left by the extracted aluminum atom in the Al surface layer after oxidation process). Site 1, with the Cu explicitly bonded to three Al atoms, is the most energetically favorable among all the sites studied here, with a binding energy of −3.58 eV (compared to −2.78 eV for Cu adsorption on perfect Al(111) surface). This bridge configuration, close to the oxide nucleus, is similar to the configuration obtained after CuO dissociative adsorption onto Al(111) (Figure 2). Adsorption site 2 is characterized by an adsorption energy of −2.92 eV and is again slightly more stable than adsorption on the pure Al(111) surface. Interestingly, in both of the above structures, the copper atoms interact with two nonoxidized Al atoms from the surface (d_{Cu-Al} = 2.41 Å) and one oxidized Al at the edge of the oxide nucleus (d_{Cu-Al} = 2.46 Å). A Bader charge analysis of site 1 shows a net charge of −1 e on the copper atom extracted from the Al atom bonded to

two oxygen atoms, evidenced by a charge variation from +1.54 to +1.87 e. This indicates that copper behaves like an oxygen atom (in the sense that it is electrophilic) in the vicinity of an oxide nucleus, which stabilizes the surface compared to an isolated copper on a pure Al(111) surface. A charge isosurface analysis of this configuration clearly shows the nature of copper behavior (see Figure 13). While the oxygen atoms share their

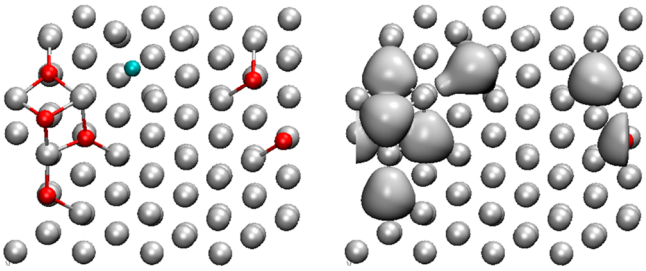

Figure 13. (Left) Top view of an oxide nucleus interacting with a copper atom. (Right) Charge density isosurface of the left side atomic arrangement (1.1 electron/Å^3). Gray, blue, and red spheres are aluminum, copper, and oxygen atoms, respectively.

electron clouds as in a perfect oxide network, the copper atom does not share its electrons with the oxygen network cloud. The aluminum atom bonded to the copper atom, and two oxygen atoms from the oxide nucleus screen this interaction, which allows the copper atom not to suffer the classical Coulombic repulsion from the oxygen negative charge. Finally, the overall stabilization of site 1 (and 2, to a lesser extent) comes from the oxygen−aluminum−copper arrangement, in which the charge reduction of the aluminum atom stabilizes the copper anion while keeping it at an optimal distance from the oxygen electron cloud. Site 1 is more stable than site 2 because it is characterized by a better orientation with respect to the bond orientation of the Al to oxide nucleus atom (tetrahedral basis).

For a single copper atom adsorbed in a second neighbor position of the nucleus, on normal hcp and fcc sites (sites 3 and 4, respectively, in Figure 12a), the adsorption energies are of −2.69 and −2.57 eV, respectively. In these sites, the trend is reversed and the Cu adsorption becomes less favorable than on the bare surface. This result may be the consequence of a modified charge environment in the vicinity of the oxide nucleus (due to the large electronegativity of oxygen atoms), causing an electronic depletion and lower adsorption energies. In addition to positions of a Cu atom around the oxide (1−4 in Figure 12), the other positions of a Cu atom on top of the oxide (position 5 in Figure 12), and below the oxide (position 6 in Figure 12) are examined. On top of the oxide (position 5), a repulsion is observed, compared to the most favorable configuration, site 1, with an enthalpy of −3.58 eV. Below the oxide, in site 6, the Cu atom is placed in an Al vacancy site formed through extraction process, leading to an enthalpy of −2.42 eV that is therefore energetically less favorable.

Finally, we examine the propensity of a Cu atom to migrate into the subsurface, focusing on the most favorable site for on top adsorption, namely site 1 in Figure 12. We find that the penetration of Cu at this site into the Al layer is energetically more favorable by 0.1 eV compared to the on top adsorption (initial surface position), as illustrated in Figure 12b, with a total enthalpy of −3.68 eV. The activation barrier for this process is 0.16 eV, according to an NEB calculation, showing that the penetration energy profile is globally similar to the one obtained on the pure Al surface. Therefore, the presence of oxide nuclei will not prevent the penetration of Cu atoms in the subsurface. In fact, the slight lowering of the energy barrier suggests that, during co-deposition, the presence of oxide on the surface will accelerate copper penetration, at least in an immediate neighborhood of the oxide nuclei.

Oxygen Reactivity on Cu-Rich Zone. In this section, we consider a Cu/Al model-surface with a large penetration of copper species in the Al(111) surface by placing an extra Cu monolayer in the first subsurface layer of the aluminum slab. There are two possible arrangements with a Cu layer separating the top Al layer from the bulk aluminum: one leads to a stacking fault of the top Al layer with respect to the bulk and the other maintains the top Al layer in registry with the bulk. We find that the latter is slightly less stable. So, we focus on the structure associated with stacking fault and call this model-structure "AlCu alloy". In general, the insertion of Cu into the subsurface is consistent with previous theoretical studies that showed that copper segregation in the Al subsurface occurs at the early stages of Al−Cu alloying.[30]

Oxygen adsorption on this modified AlCu alloy surface shows slightly different features with respect to oxygen adsorption on pure Al(111) surfaces. The fcc sites are still preferential with respect to hcp sites, but the energy difference is reduced to 0.2 eV (E_{ads}(fcc) = −7.80 eV and E_{ads}(hcp) = −7.60 eV), compared to 0.4 eV in the case of pure Al(111) surface (see section 3). We also observe a small shift in the adsorption energy: from −7.64 eV for pure Al to −7.80 eV for AlCu alloy in the fcc site. This leads to a stronger binding of oxygen on the AlCu alloy, probably due to the distortions associated with Cu insertion, facilitating the breakdown of the Al lattice structure and further interaction toward incoming oxygen atoms.

In Figure 14, we represent the incremental binding energies of oxygen atoms deposited on this AlCu alloy, calculated as in

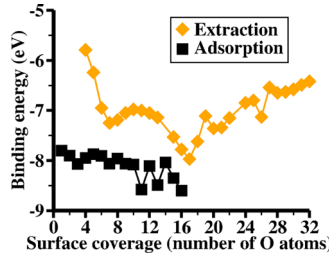

Figure 14. Extraction (orange ◆) vs adsorption (black ■) binding energies as a function of the oxygen surface coverage, for the AlCu alloy. Oxygen adsorption curve is stopped at 16 O atoms because a full monolayer is reached at this stage.

Figure 10 on pure aluminum. By comparing Figures 10 and 14, we observe similar features, up to 1 ML oxygen coverage, with the adsorption remaining more favorable than extraction. Continuing with this comparison, we observe that the extraction mechanism is also easier in the presence of Cu in the subsurface, as for the adsorption. Here, the energy differences are systematically lower on the AlCu alloy substrate (average 0.14 eV energy gain). However, all these calculations only concern the adsorption of one single oxygen atom above the first adsorbed oxygen layer. For an oxygen coverage over 1 ML, the incoming oxygen atoms inevitably form oxygen clusters in the second oxygen layer. Therefore, oxygen

clustering effects can no longer be ignored. In our procedure, we systematically consider close-packed oxygen atoms in the second layer. At such high coverage, the extraction of aluminum is affected. While the energy to extract Al decreases with increasing oxygen coverage on pure Al, this extraction energy begins to increase with oxygen coverage above 1 ML for the AlCu alloy. Concomitantly, the binding energy of oxygen on AlCu alloy decreases slightly with increasing oxygen coverage (Table 3). The oxidation is still exothermic but is more difficult with increasing coverage. Figure 14 indicates that the incremental extraction energy starts increasing after deposition of two extra oxygen atoms on the first full oxygen layer (corresponding to 18 oxygen atoms in the unit cell), forming a small oxide cluster. In effect, the formation of oxygen clusters, even of small sizes, in the second oxygen layer leads to the extraction of a number of surface Al atoms with associated lattice distortion, which allows Cu atoms to be located immediately below the oxygen atoms.

Table 3. Extraction Energies as a Function of Oxygen Coverage for Three Model-Systems: Pure Aluminum, AlCu Alloy, and AlCu Alloy with Copper Layer Located in the Second Subsurface Layer

	number of O atoms			
	17	18	19	20
on pure Al	−7.46	−7.45	−7.21	−7.60
on AlCu alloy	−7.97	−7.62	−7.10	−7.35
Cu on the second subsurface layer	−8.81	−8.81	−8.94	−9.8

As discussed in a previous subsection, copper and oxygen atoms have a tendency to repel each other due to their electronegativity. We therefore propose that as Cu finds itself next to oxygen due to Al extraction, there will be a driving force for migration of these Cu atoms from the first subsurface layer to the second subsurface layer during the oxidation process. Although this assumption has not been checked in full detail (i.e., with kinetic calculations of the activation energy barriers for this migration mechanism), we have tested the special cases with Cu in subsurface layers. If Cu is deliberately placed in the second instead of the first subsurface layer, there is a notable gain of energy. Associated with this energy gain, the energy for aluminum extraction is also reduced compared to the extraction energy for Cu in the first subsurface layer (Table 3). In Figure 15, we show the simulation results of structures obtained after the deposition of 19 oxygen atoms on both model surfaces (Cu in first and second subsurface layers). The left side of Figure 15 shows that the overall interfacial layer is distorted; the copper layer positioned at the first subsurface layer the aluminum layer underneath are disorganized. In contrast, the right side shows that the copper layer now in the second subsurface layer is stable. Importantly, the aluminum layer is now situated just under the oxide nucleus allowing the formation of an additional Al−O bond, which increases the total energy of this system substantially. This stabilization effect is shown in Table 3, in going from 17 to 20 oxygen atoms. Therefore, the presence of copper enhances the oxidation of aluminum, as long as the Cu atoms are not in direct (or too close) contact with oxygen atoms. Consequently, there is a driving force to push Cu atoms toward the bulk as oxidation proceeds. This mechanism is likely not spontaneous but thermally activated, although the details of this mechanism (e.g., activation barriers) need to be further investigated.

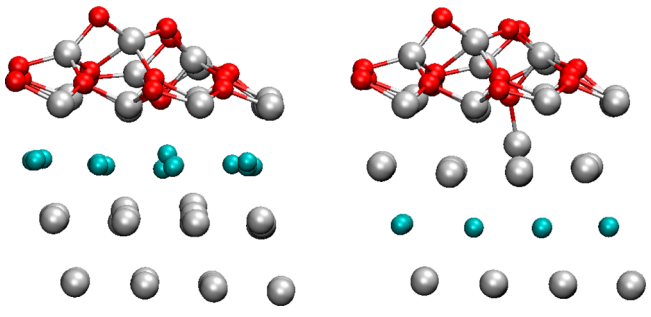

Figure 15. Extraction processes on two different AlCu alloys with 19 oxygen atoms deposited. (Left) The AlCu alloy has its copper layer situated on the first subsurface layer. (Right) The copper layer is placed in the second subsurface layer. Gray, blue, and red spheres are aluminum, copper, and oxygen atoms, respectively.

CONCLUSION

In summary, the deposition of CuO on an Al(111) surface has been investigated by DFT-based calculations, using a six-layer Al slab model. We first find that copper monoxide is always dissociated when deposited on an Al(111) surface, thus making the separate studies of the adsorption of atomic copper and oxygen relevant. We then observe that Cu atoms are adsorbed with similar energies on hcp and fcc sites, consistent with previous studies. We also show that adsorbed Cu atoms are highly mobile on the surface. As a result of their rapid migration, Cu atoms tend to form islands on the surface. Further, we find that Cu atoms can easily penetrate into the Al subsurface, particularly upon clustering, which lowers the penetration activation barrier, creating Al adatoms on the surface. These characteristics explain the experimentally observed rapid penetration of copper deposited on aluminum, leading to an intermixing of the two species.[46−48]

Oxygen adsorption on aluminum is very exothermic, preferentially occupying the fcc sites, in agreement with literature. The migration barriers are such that they promote occupation of fcc rather than hcp sites at room temperature. We provide evidence for oxygen clustering as the energy barrier to detach an oxygen atom from a cluster increases with the cluster size, which explains the experimentally observed cluster formation.[43,49] These findings confirm that, at finite temperatures, oxygen atoms can migrate and form clusters that remain stable over time. Furthermore, we show that oxygen penetration into the surface is kinetically forbidden, forcing adsorbed oxygen (1 × 1) islands to remain on the surface. The presence of these oxygen clusters is the seed for a new mechanism, called extraction, which leads to aluminum oxidation. This extraction mechanism is exothermic and barrierless. It involves an oxygen atom deposited on top of an existing oxygen (1 × 1) cluster, fostering the extraction of three Al atoms out of their lattice sites and forming a stable oxide nucleus standing above the original oxygen (1 × 1) cluster.[37] Further addition of oxygen atoms up to 2 ML coverage leads to an oxide structure with a local symmetry similar to γ-Al_2O_3, consistent with previous experimental studies.[61−63]

Finally, the copper and oxygen behavior relative to oxygen- and copper-rich zones of the aluminum surface, respectively, have been considered, because it is relevant during CuO deposition at high surface coverages. Our aim has been to

understand the formation of mixed layers, together with their structure and composition, in the final multilayer nanothermites. On one hand, we find that the presence of oxide on the surface facilitates the adsorption and insertion of copper in its direct neighborhood. On the other hand, the presence of Cu in the subsurface enhances the oxygen adsorption on Al(111) surfaces. These two effects enhance Al extraction right above regions with subsurface Cu, which is found to increase up to 1 oxygen ML. At higher oxygen coverage, after oxidation has depleted the Al subsurface layer, the repulsion between oxygen and copper fosters the migration of Cu deeper into the Al substrate, preventing full Cu, O, and Al mixing. Instead, there is aluminum oxide formation and copper condensation. Therefore, these DFT calculations have shown that there is not a formation of a classical ternary compound with Al, O, and Cu intermixed, but initial oxygen and copper clustering and later segregation into aluminum oxide and copper condensation in the bulk. The present description of the evolution of this complex system, under well-defined experimental conditions, cannot be easily deduced from empirical considerations. While the present theoretical studies shed light on the essential elementary processes, there is still a need for the detailed DFT-based Kinetic Monte Carlo simulations, currently in progress, to develop an understanding complete enough to control the full CuO deposition process on aluminum.

Importantly, this work represents the first fundamental study of elementary processes associated with the widely used Al−Cu alloy, providing a new paradigm for the initial oxidation mechanism based on the subtle interplay of cluster formation, aluminum extraction and copper condensation in subsurface regions.

AUTHOR INFORMATION

Corresponding Author

*E-mail: aesteve@laas.fr. Phone: 33 5 61 33 63 53.

Notes

The authors declare no competing financial interest.

ACKNOWLEDGMENTS

This work has been performed using CALMIP computer resources (GRANT 1033). It has been supported by the ANR-NSF CIREN (NSF-DMR-1312525), VIMA-RTRA project, DGA-REI (2009340047), and the CNRS LIA-ATLAB initiative.

REFERENCES

(1) Rossi, C.; Zhang, K.; Esteve, D.; Alphonse, P.; Tailhades, P.; Vahlas, C. Nanoenergetic Materials for Mems: A Review. *J. Microelectromech. Syst.* **2007**, *16*, 919−931.

(2) Zhang, K.; Rossi, C.; Rodriguez, G. A. A.; Tenailleau, C.; Alphonse, P. Development of a Nano-Al/CuO Based Energetic Material on Silicon Substrate. *Appl. Phys. Lett.* **2007**, *91*, 113117.

(3) Rossi, C.; Esteve, A.; Vashishta, P. Nanoscale Energetic Materials. *J. Phys. Chem. Solids* **2010**, *71*, 57−58.

(4) Petrantoni, M.; Rossi, C.; Salvagnac, L.; Conedera, V.; Esteve, A.; Tenailleau, C.; Alphonse, P.; Chabal, Y. J. Multilayered Al/CuO Thermite Formation by Reactive Magnetron Sputtering: Nano Versus Micro. *J. Appl. Phys.* **2010**, *108*, 084323.

(5) Petrantoni, M.; Rossi, C.; Conedera, V.; Bourrier, D.; Alphonse, P.; Tenailleau, C. Synthesis Process of Nanowired Al/CuO Thermite. *J. Phys. Chem. Solids* **2010**, *71*, 80−83.

(6) Zhang, K. L.; Rossi, C.; Petrantoni, M.; Mauran, N.; Nano, A. Initiator Realized by Integrating Al/CuO-Based Nanoenergetic Materials with a Au/Pt/Cr Microheater. *J. Microelectromech Syst* **2008**, *17*, 832−836.

(7) Blobaum, K. J.; Reiss, M. E.; Lawrence, J. M. P.; Weihs, T. P. Deposition and Characterization of a Self-Propagating CuO_x/Al Thermite Reaction in a Multilayer Foil Geometry. *J. Appl. Phys.* **2003**, *94*, 2915−2922.

(8) Blobaum, K. J.; Wagner, A. J.; Plitzko, J. M.; Van Heerden, D.; Fairbrother, D. H.; Weihs, T. P. Investigating the Reaction Path and Growth Kinetics in CuO_x/Al Multilayer Foils. *J. Appl. Phys.* **2003**, *94*, 2923−2929.

(9) Manesh, N. A.; Basu, S.; Kumar, R. Experimental Flame Speed in Multi-Layered Nano-Energetic Materials. *Combust. Flame* **2010**, *157*, 476−480.

(10) Zhu, P.; Shen, R. Q.; Ye, Y. H.; Zhou, X.; Hu, Y. Energetic Igniters Realized by Integrating Al/CuO Reactive Multilayer Films with Cr Films. *J. Appl. Phys.* **2011**, *110*, 074513.

(11) Kwon, J.; Ducere, J. M.; Alphonse, P.; Bahrami, M.; Petrantoni, M.; Veyan, J. F.; Tenailleau, C.; Esteve, A.; Rossi, C.; Chabal, Y. J. Interfacial Chemistry in Al/CuO Reactive Nanomaterial and Its Role in Exothermic Reaction. *ACS Appl. Mater. Interfaces* **2013**, *5*, 605−613.

(12) Hemeryck, A.; Petrantoni, M.; Esteve, A.; Rossi, C.; Djafari Rouhani, M.; Landa, G.; Esteve, D. A Mesoscopic Model of the Intermixing During Nanoenergetic Materials Processing. *J. Phys. Chem. Solids* **2010**, *71*, 125−129.

(13) Hemeryck, A.; Ducere, J. M.; Lanthony, C.; Esteve, A.; Rossi, C.; Djafari-Rouhani, M.; Esteve, D. Bottom-Up Modeling of Al/Ni Multilayer Combustion: Effect of Intermixing and Role of Vacancy Defects on the Ignition Process. *J. Appl. Phys.* **2013**, *113*, 204301.

(14) Politano, O.; Baras, F.; Mukasyan, A. S.; Vadchenko, S. G.; Rogachev, A. S. Microstructure Development During Nial Intermetallic Synthesis in Reactive Ni-Al Nanolayers: Numerical Investigations vs TEM Observations. *Surface & Coatings Technology* **2013**, *215*, 485−492.

(15) Taylor, T. N.; Martin, J. A. Reaction of Vapor-Deposited Aluminum with Copper Oxides. *J. Vac. Sci. Technol., A* **1991**, *9*, 1840−1846.

(16) Alawieh, L.; Knio, O. M.; Weihs, T. P. Effect of Thermal Properties on Self-Propagating Fronts in Reactive Nanolaminates. *J. Appl. Phys.* **2011**, *110*, 013509.

(17) Gavens, A. J.; Van Heerden, D.; Mann, A. B.; Reiss, M. E.; Weihs, T. P. Effect of Intermixing on Self-Propagating Exothermic Reactions in Al/Ni Nanolaminate Foils. *J. Appl. Phys.* **2000**, *87*, 1255−1263.

(18) Blobaum, K. J.; Van Heerden, D.; Wagner, A. J.; Fairbrother, D. H.; Weihs, T. P. Sputter-Deposition and Characterization of Paramelaconite. *J. Mater. Res.* **2003**, *18*, 1535−1542.

(19) Amini-Manesh, N.; Basu, S.; Kumar, R. Modeling of a Reacting Nanofilm on a Composite Substrate. *Energy* **2011**, *36*, 1688−1697.

(20) Gan, Y.; Chen, Z.; Gangopadhyay, K.; Bezmelnitsyn, A.; Gangopadhyay, S. An Equation of State for the Detonation Product of Copper Oxide/Aluminum Nanothermite Composites. *J. Nanopart. Res.* **2010**, *12*, 719−726.

(21) Zhao, S. J.; Germann, T. C.; Strachan, A. Atomistic Simulations of Shock-Induced Alloying Reactions in Ni/Al Nanolaminates. *J. Chem. Phys.* **2006**, *125*, 164707.

(22) Zhao, S. J.; Germann, T. C.; Strachan, A. Melting and Alloying of Ni/Al Nanolaminates Induced by Shock Loading: A Molecular Dynamics Simulation Study. *Phys. Rev. B* **2007**, *76*, 104105.

(23) Baras, F.; Politano, O. Molecular Dynamics Simulations of Nanometric Metallic Multilayers: Reactivity of the Ni-Al System. *Phys. Rev. B* **2011**, *84*, 024113.

(24) Linde, A.; Politano, O.; Baras, F. Study of the Reactive Dynamics of Nanometric Metallic Multilayers Using Molecular Dynamics: The Al−Ni System. In *Diffusion in Materials—DIMAT 2011*; Bezverkhyy, I., Chevalier, S., Politano, O., Eds.; Defect and Diffusion Forum, 2012; pp 89−94.

(25) Petrantoni, M.; Hemeryck, A.; Ducere, J. M.; Esteve, A.; Rossi, C.; Rouhani, M. D.; Esteve, D.; Landa, G. Asymmetric Diffusion as a

Key Mechanism in Ni/Al Energetic Multilayer Processing: A First Principles Study. *J. Vac. Sci. Technol., A* **2010**, *28*, L15−L17.
(26) Shimojo, F.; Nakano, A.; Kalia, R. K.; Vashishta, P. Electronic Processes in Fast Thermite Chemical Reactions: A First-Principles Molecular Dynamics Study. *Phys. Rev. E* **2008**, *77*, 066103.
(27) Shimojo, F.; Nakano, A.; Kalia, R. K.; Vashishta, P. Enhanced Reactivity of Nanoenergetic Materials: A First-Principles Molecular Dynamics Study Based on Divide-and-Conquer Density Functional Theory. *Appl. Phys. Lett.* **2009**, *95*, 043114.
(28) Wadley, H. N. G.; Zhou, A. X.; Johnson, R. A.; Neurock, M. Mechanisms, Models, and Methods of Vapor Deposition. *Prog. Mater. Sci.* **2001**, *46*, 329−377.
(29) Lanthony, C.; Ducere, J. M.; Esteve, A.; Rossi, C.; Djafari-Rouhani, M. Formation of Al/CuO Bilayer Films: Basic Mechanisms through Density Functional Theory Calculations. *Thin Solid Films* **2012**, *520*, 4768−4771.
(30) Benali, A.; Lacaze-Dufaure, C.; Morillo, J. Density Functional Study of Copper Segregation in Aluminum. *Surf. Sci.* **2011**, *605*, 341−350.
(31) Perdew, J. P.; Burke, K.; Ernzerhof, M. Generalized Gradient Approximation Made Simple. *Phys. Rev. Lett.* **1996**, *77*, 3865−3868.
(32) Kresse, G.; Furthmuller, J. Efficient Iterative Schemes for Ab Initio Total-Energy Calculations Using a Plane-Wave Basis Set. *Phys. Rev. B* **1996**, *54*, 11169−11186.
(33) Kresse, G.; Furthmuller, J. Efficiency of Ab Initio Total Energy Calculations for Metals and Semiconductors Using a Plane-Wave Basis Set. *Comput. Mater. Sci.* **1996**, *6*, 15−50.
(34) Kresse, G.; Hafner, J. Ab Initio Molecular-Dynamics for Liquid-Metals. *Phys. Rev. B* **1993**, *47*, 558−561.
(35) Kresse, G.; Hafner, J. Ab Initio Molecular-Dynamics Simulation of the Liquid-Metal Amorphous-Semiconductor Transition in Germanium. *Phys. Rev. B* **1994**, *49*, 14251−14269.
(36) Monkhorst, H. J.; Pack, J. D. Special Points for Brillouin-Zone Integrations. *Phys. Rev. B* **1976**, *13*, 5188−5192.
(37) Lanthony, C.; Ducere, J. M.; Rouhani, M. D.; Hemeryck, A.; Esteve, A.; Rossi, C. On the Early Stage of Aluminum Oxidation: An Extraction Mechanism Via Oxygen Cooperation. *J. Chem. Phys.* **2012**, *137*, 094707.
(38) Guo, J. X.; Wei, L. J.; Ge, D. Y.; Guan, L.; Wang, Y. L.; Liu, B. T. Dissociation and Reconstruction of O_2 on Al (111) Studied by First-Principles. *Appl. Surf. Sci.* **2013**, *264*, 247−254.
(39) Henkelman, G.; Uberuaga, B. P.; Jonsson, H. A Climbing Image Nudged Elastic Band Method for Finding Saddle Points and Minimum Energy Paths. *J. Chem. Phys.* **2000**, *113*, 9901−9904.
(40) Henkelman, G.; Uberuaga, B. P.; Jonsson, H. Methods for Finding Saddle Points and Minimum Energy Paths. In *Theoretical Methods in Condensed Phase Chemistry*; Schwartz, S. D., Ed.; Kluwer Academic Publishers: Boston, 2000.
(41) Sheppard, D.; Terrell, R.; Henkelman, G. Optimization Methods for Finding Minimum Energy Paths. *J. Chem. Phys.* **2008**, *128*, 134106.
(42) Kerkar, M.; Fisher, D.; Woodruff, D. P.; Cowie, B. Adsorption Site Determination for Oxygen on Al(111) Using Normal Incidence Standing X-Ray Wave-Field Absorption. *Surf. Sci.* **1992**, *271*, 45−56.
(43) Brune, H.; Wintterlin, J.; Trost, J.; Ertl, G.; Wiechers, J.; Behm, R. J. Interaction of Oxygen with Al(111) Studied by Scanning-Tunneling-Microscopy. *J. Chem. Phys.* **1993**, *99*, 2128−2148.
(44) Trost, J.; Brune, H.; Wintterlin, J.; Behm, R. J.; Ertl, G. Interaction of Oxygen with Al(111) at Elevated Temperatures. *J. Chem. Phys.* **1998**, *108*, 1740−1747.
(45) Jacobsen, J.; Hammer, B.; Jacobsen, K. W.; Norskov, J. K. Electronic-Structure, Total Energies, and STM Images of Clean and Oxygen-Covered Al(111). *Phys. Rev. B* **1995**, *52*, 14954−14962.
(46) Asonen, H.; Barnes, C. J.; Salokatve, A.; Pessa, M. The Effect of Interdiffusion on the Growth Mode of Copper on Al(111). *Surf. Sci.* **1985**, *152* (Apr), 262−269.
(47) Barnes, C. J.; Asonen, H.; Salokatve, A.; Pessa, M. Growth Mode and Electronic-Structure of Copper-Films on Aluminum Substrates. *Surf. Sci.* **1987**, *184*, 163−176.
(48) Buchanan, J. D. R.; Hase, T. P. A.; Tanner, B. K.; Chen, P. J.; Gan, L.; Powell, C. J.; Egelhoff, W. F. Anomalously Large Intermixing in Aluminum-Transition-Metal Bilayers. *Phys. Rev. B* **2002**, *66*, 104427.
(49) Brune, H.; Wintterlin, J.; Behm, R. J.; Ertl, G. Surface Migration of Hot Adatoms in the Course of Dissociative Chemisorption of Oxygen on Al(111). *Phys. Rev. Lett.* **1992**, *68*, 624−626.
(50) Katz, G.; Kosloff, R.; Zeiri, Y. Abstractive Dissociation of Oxygen over Al(111): A Nonadiabatic Quantum Model. *J. Chem. Phys.* **2004**, *120*, 3931−3948.
(51) Ciacchi, L. C.; Payne, M. C. "Hot-Atom" O_2 Dissociation and Oxide Nucleation on Al(111). *Phys. Rev. Lett.* **2004**, *92*, 176104.
(52) Yourdshahyan, Y.; Razaznejad, B.; Lundqvist, B. I. Adiabatic Potential-Energy Surfaces for Oxygen on Al(111). *Phys. Rev. B* **2002**, *65*, 075416.
(53) Carbogno, C.; Behler, J.; Reuter, K.; Gross, A. Signatures of Nonadiabatic O_2 Dissociation at Al(111): First-Principles Fewest-Switches Study. *Phys. Rev. B* **2010**, *81*, 035410.
(54) Zhukovskii, Y. F.; Jacobs, P. W. M.; Causa, M. On the Mechanism of the Interaction between Oxygen and Close-Packed Single-Crystal Aluminum Surfaces. *J. Phys. Chem. Solids* **2003**, *64*, 1317−1331.
(55) Frederick, B. G.; Lee, M. B.; Richardson, N. V. A Vibrational Characterisation of the O/A1(111) System: A Reassignment of HREELS Data. *Surf. Sci.* **1996**, *348* (3), L71−L74.
(56) Neuburger, M. L.; Pullman, D. P. On the Viability of Single Atom Abstraction in the Dissociative Chemisorption of O_2 on the Al(111) Surface. *J. Chem. Phys.* **2000**, *113*, 1249−1257.
(57) Kiejna, A.; Lundqvist, B. I. First-Principles Study of Surface and Subsurface O Structures at Al(111). *Phys. Rev. B* **2001**, *63*, 085405.
(58) Kiejna, A.; Lundqvist, B. I. Stability of Oxygen Adsorption Sites and Ultrathin Aluminum Oxide Films on Al(111). *Surf. Sci.* **2002**, *504*, 1−10.
(59) Chakarova, R.; Oner, D. E.; Zoric, I.; Kasemo, B. Monte Carlo Simulation of Initial Al(111) Oxidation. *Surf. Sci.* **2001**, *472*, 63−79.
(60) Jiang, K. Y.; Music, D.; Sarakinos, K.; Schneider, J. M. Ab Initio Study of Effects of Substitutional Additives on the Phase Stability of Gamma-Alumina. *J. Phys.: Condens. Matter* **2010**, *22*, 505502.
(61) Jennison, D. R.; Verdozzi, C.; Schultz, P. A.; Sears, M. P. Ab Initio Structural Predictions for Ultrathin Aluminum Oxide Films on Metallic Substrates. *Phys. Rev. B* **1999**, *59*, 15605−15608.
(62) Reichel, F.; Jeurgens, L. P. H.; Richter, G.; Mittemeijer, J. Amorphous Versus Crystalline State for Ultrathin Al_2O_3 Overgrowths on Al Substrates. *J. Appl. Phys.* **2008**, *103* (9), 093515.
(63) Jeurgens, L. P. H.; Sloof, W. G.; Tichelaar, F. D.; Mittemeijer, E. J. Structure and Morphology of Aluminium-Oxide Films Formed by Thermal Oxidation of Aluminium. *Thin Solid Films* **2002**, *418* (2), 89−101.